TELKOMNIKA Indonesian Journal of Electrical Engineering
Vol.12, No.2, February 2014, pp. 1577 ~ 1584
DOI: http://dx.doi.org/10.11591/telkomnika.v12i2.3623

Maximum Value Search and Polynomial Fit Metal Artifact Reduction Algorithm

Li yuanjin*, Wang tao
Department of Computer, Chuzhou University, Chuzhou, 239000, China
*Corresponding author, e-mail: liyuanjin11@126.com

Abstract

Metal artifacts seriously degrade CT image quality, and even restrict the using of computed tomography imaging. In this paper, the authors propose a metal artifact reduction algorithm to suppress the metal artifacts in CT image. The metal artifact reduction algorithm, in this paper, includes six steps: coarse metal implant segmentation, nearly accurate metal object segmentation, forward projection, polynomial-based fit, adaptive scaling as well as final image reconstruction. Experiment on image showed that RMSEs between the corrected image using polynomial fit, nearest interpolation, linear interpolation and spline interpolation and ideal model image are 0.20912, 0.33252, 0.24257 and 0.26791, respectively. It has the potential to greatly improve the quality of CT image and suppress the metal artifacts.

Keywords: *nearly accurate metal object segmentation, polynomial-based fit, metal artifact reduction, metal artifact reduction algorithm, adaptive scaling*

1. Introduction

Computed tomography (CT) imaging is one of the most established techniques for medical diagnosis assistance [1]. Nevertheless, with the presence of metal objects in the field of view (FOV), such as dental implants and internal fixation, some metal artifacts emerge in the reconstructed CT image using the raw projection data. The metal artifacts seriously affect the diagnosis of cross-section structure and greatly deteriorate CT image quality, and further hardly possible attain the goal of nondestructive detect and medical treatment diagnosis. Thus people require some efficient methods to reduce or suppress, and even remove the metal artifacts from the reconstructed CT image.

Many metal artifact reduction (MAR) methods [1-14], [18,19] have been studied and published. On the whole, they can be classified into two types: physical methods and software methods. Physical methods again include replacing the metal implants with less attenuating coefficient materials, installing thinner and smaller cross-section [2-5] or using the higher energy X-ray beam. As we all know that higher energy X-ray beam harms people healthiness and the metal implants with higher attenuation coefficient in the body can't be replace with less attenuating coefficient materials because they have existed in the body before scanning. Thus physical methods are unpractical and can't be realized. As a result, people more seek to software methods solve the problem. Generally speaking, software methods are classified into three different groups: interpolation corrections approaches [6-10], iterative reconstruction approaches [11-13] and hybrid approaches. Interpolation method consists of the following steps: coarse image reconstruction, metal object segmentation, forward projection, projection interpolation, final image reconstruction and metal compensation. The biggest virtue of the method is simple and computationally efficient. What's more, they can effectively suppress a number of metal artifacts. But secondary artifacts are the fatal shortcomings of the type of method. As far as iterative metal artifact reduction methods [11-13], they can achieve better image quality than interpolation methods. However, they are computationally expensive and difficult to implement in current CT scanners. Due to the high efficacy of interpolation methods and better image quality of iterative methods, people propose hybrid approaches for metal artifact reduction problem. Though the published algorithms seem to promising, none of them has been found wide acceptance in commercial CT scanners.

Received June 24, 2013; Revised September 4, 2013; Accepted October 7, 2013

In this paper, the authors propose a novel MAR algorithm based on maximum value search and polynomial fit to suppress the metal artifacts in CT image. The most major characteristic of the proposed algorithm is that the maximum value searching and polynomial fit method are firstly proposed by the authors to reduce the metal artifacts.

2. Materials and Methods

Before further elaborating the novel algorithm for MAR, the authors suppose that all images shown in the paper are pre-processed with a dedicated ring artifacts correction method [14] to improve the accuracy of detecting metal objects in the CT image.

In this paper, the metal artifact reduction method includes six steps: coarse metal object segmentation, nearly accurate metallic object segmentation, forward projection, polynomial-based fit filling, adaptive scaling and filtering as well as final image reconstruction.

2.1. Coarse Identification of Metal Image Region

To minimize the effect of mistakenly detecting artifacts as metal object, firstly, the uncorrected cross-section 2D CT image is smoothed by performing the low-pass filter to reduce high-frequency artifacts. The chosen filter is a 2D Gaussian filter [15], with a 5 by 5 pixel mask and a standard deviation of 1. In references [16], Abdolvahab Ehsani Rad proposed level-set method to segmeent digital dental X-Ray image. Jun Lai presented automatic segmentation for pulmonary vessls in plain thoracic CT Scans [17]. To shorten the time, the proposed method plots the gray intensities histogram of 2D CT image, by which metal image region in 2D CT image is coarsely segmented.

2.2. Nearly Accurate Metallic Object Segmentation

Due to the impossible character of absolutely accurate metal object segmentation, the authors propose nearly accurate metal object segmentation region-based maximum value search. As we all know, the gray intensities of a material differ very little, but different materials may have very greatly different gray intensities. According to the fact, the authors segment the metal object from the coarse identification of metal image region. The following shows the process of the algorithm.

Step 1: Finding the maximal gray intensity $V_{\max}$ of the coarsely segmented metal image. If some regions have some local maximal gray intensity $V_{l\max}$ and haven't maximal gray intensity $V_{\max}$. Then the authors propose $V_{l\max}$ as $V_{\max}$ if the difference between $V_{l\max}$ and $V_{\max}$ is very little.

Step 2: Supposing the maximal proportion T_0, and the minimal proportion T_1.Of course, the T_0 and T_1 ought to be acquired by all times experiments.

Step 3: The algorithm itself starts from the location of the maximal gray intensity $V_{\max}$ or local maximal gray intensity $V_{l\max}$, and adds it to the metal object region, and then searches the gray intensity V of 4-connected neighborhood or 8-connected neighborhood, and judges the following formula:

$$T_1 < \left| \frac{V}{V_{\max}} \right| < T_0 \quad (1)$$

Step 4: If formula (1) is yes, the algorithm adds V to the metal object region, and then searches the gray intensity V_1 of its 4-connected neighborhood or 8-connected neighborhood. Assigning V to $V_{\max}$, V_1 to V, judging the formula (1).

Step 5: Repeating step 4 until it is no.

The authors combine the above algorithm with the watershed value of a fixed fraction of the maximum value [18] nearly accurately segment the metal object from the coarse identification of metal image region.

2.3. Forward Projection

After the authors obtain the coarse identification of metal image region and nearly accurately segment the metal object, forward projections are done to acquire their projection data. Here the authors use the parallel model to transform the uncorrected 2D CT image into parallel beam projection data $p(m_1, n_1), m_1 = 1,..., M; n_1 = 1,..., N$. Accordingly the nearly accurately segmented metal object projects into $p(m_2, n_2), m_2 = 1,..., M; n_2 = 1,..., N$. Where M is the total number of detectors and N is the total number of projection views. The accurate positions of metal object under each projection view can be determined:

$$R(i, j) = \{[s_{i,j}, e_{i,j}]\}, i = 1,..., M; j = 1,..., i(k) \quad (2)$$

Where $i(k)$ is the total number of metal regions in the ith row, $s_{i,j}$ and $e_{i,j}$ denote the jth metal regions starting and ending in the ith row, respectively.

2.4. Polynomial-based Fit Filling

Interpolation method means to construct a function that passes through a group of given points. But the raw projection data inevitably have some errors, and interpolation function includes the errors. Thus the authors propose a method with the name of least square polynomial fit to solve the problem. The goal of the least square polynomial fit, in the paper, eliminates the inconsistent part in the image caused by missing or incomplete projection data.

Let $(x_i, y_i)(i = 0,1,..., m)$ be a group given points of a row in the projection. A set of functions of less than $n\ (n \le m)$ times polynomial Φ is made up. Looking for $p_n(x) = \sum_{k=0}^{n} a_k x^k \in \Phi$, which makes:

$$I = \sum_{i=0}^{m} [p_n(x_i) - y_i]^2 = \sum_{i=0}^{m} (\sum_{k=0}^{n} a_k x_i^k - y_i)^2 = \min \quad (3)$$

Here min implies least. $p_n(x)$ is known as least square fit polynomial if it meets with formula (3). It is apparent that $I = \sum_{i=0}^{m} (\sum_{k=0}^{n} a_k x^k - y_i)^2$ is a multifunction of coefficients $a_0, a_1,..., a_n$. According to the essential condition of solving extreme value of the multifunction,

$$\frac{\partial I}{\partial a_j} = 2\sum_{i=0}^{m} (\sum_{k=0}^{n} a_k x_i^k - y_i) x_i^j = 0, \quad j = 0,1,..., n \quad (4)$$

Namely,

$$\sum_{k=0}^{n} (\sum_{i=0}^{m} x_i^{j+j}) a_k = \sum_{i=0}^{m} x_i^j y_i, \qquad j = 0,1,..., n \quad (5)$$

Formula (5) is linear equation of coefficients and (6) is its matrix format.

$$\begin{bmatrix} m+1 & \sum_{i=0}^{m} x_i & ... & \sum_{i=0}^{m} x_i^n \\ \sum_{i=0}^{m} x_i & \sum_{i=0}^{m} x_i^2 & ... & \sum_{i=0}^{m} x_i^{n+1} \\ . & . & . & . \\ \sum_{i=0}^{m} x_i^n & \sum_{i=0}^{m} x_i^{n+1} & ... & \sum_{i=0}^{m} x_i^{2n} \end{bmatrix} \begin{bmatrix} a_0 \\ a_1 \\ ... \\ a_n \end{bmatrix} = \begin{bmatrix} \sum_{i=0}^{m} y_i \\ \sum_{i=0}^{m} x_i y_i \\ ... \\ \sum_{i=0}^{m} x_i^n y_i \end{bmatrix} \quad (6)$$

From formula (6) $a_0, a_1, ..., a_n$ can be solved. So the following polynomial $p_n(x)$ can be obtained:

$$p_n(x) = \sum_{k=0}^{n} a_k x^k \in \Phi \quad (7)$$

According to formula (7) and the column coordinates of every row in the corrupt projection region, the every point value of the corrupted projection region can be calculated, and then is inserted in the corrupted projection region.

2.5. Adaptive Scaling

After the last polynomial fit step, a base profile $b(m_1, n_1)$ which corresponds to the baseline sinogram described by Chen etc [19] is formed for all regions in $R(i, j)$. Thus the measured profile of the metal objects can be calculated by the following formula.

$$p_m(m_1, n_1) = p(m_1, n_1) - b(m_1, n_1), m_1 = 1,..., M; n_1 = 1,..., N \quad (8)$$

After the metal sinogram is obtained, an adaptive scaling and filtering step are used to suppress the metal artifacts and preserve the information of metal parts in detail [19]. The scaling is applied on $p_m(m_1, n_1)$ defined by:

$$p_m^{'}(m_1, n_1) = k * p_m(m_1, n_1), \quad (9)$$

The coefficient k is between 0.3 and 0.5 [19].

2.6. Final Image Reconstruction

After the raw metal projection data have already been modified by the above several steps, they can be integrated by adding polynomial fit data to adaptive scaling data into a corrected metal projection. All raw projection data outside of the metal projection regions are kept unchanged. Namely:

$$p_c = \begin{cases} p(m_1, n_1) & p_c \in p(m_1, n_1) \text{ and } p_c \notin R(i, j) \\ b(m_1, n_1) + p_m^{'}(m_1, n_1) & p_c \in R(i, j) \end{cases} \quad (10)$$

Where p_c is the corrected projection data. Finally, the corrected projection data are fed into a filtered back projection procedure as usual to reconstruct the final metal artifacts reduced image.

3. Validation and Feasibility of the New Framework

3.1. Simulative Data Acquisition

To demonstrate the validation and feasibility of the proposed MAR algorithm, the authors experiment on it using Visual Studio 2005 and MATLAB R2007 on PC with 1.00GB memory and 1.5GHz CPU to the 3D phantom. Table 1 shows the parameter values of the 3D phantom.

Table 1. Normalized parameters of the phantom for numerical simulation

n	a	b	c	x	y	z	θ°	ρ
1	0.960	0.850	0.920	0.0	0.0	0.0	0.0	4.0
2	0.350	0.250	0.250	0.0	0.2	0.1	0.0	1.5
3	0.350	0.250	0.250	0.0	0.2	-0.1	0.0	-1.5
4	0.075	0.075	0.075	-0.705	0.0	-0.25	0.0	53.5
5	0.075	0.075	0.075	0.705	0.0	-0.25	0.0	53.5

Where:

n denotes the number of ellipsoids; a, b, c are the lengths of three semi-axes of each ellipsoid, respectively; x, y, z show the central coordinates of ellipsoid; θ° is the rotation angle; ρ is the attenuation coefficient

3.2. Algorithm Implementation Course

As shown in Figure 1, a whole processes can be seen using the proposed method in this paper. Figure 1(a) serves as an idea model without any artifacts and noises. Figure 1(b) with severe streak artifacts in the 2D CT image is caused by the two simulative metal objects in the phantom before corrections are applied. Figure 1(c) is filtered 2D CT image. Here 2D CT image is a cross-section of 3D image. The histogram is shown in the Figure 1(c) and Figure. 1(d) coarsely segmented image with threshold 170. Figure 1(e) is the result of nearly accurate segmentation. Figure 1(f) shows the final corrected CT image (k=0.3)using the proposed approach in this paper.

Figure 2 shows the corrected images with nearest interpolation, linear interpolation and spline interpolation ($k = 0.3$).Compared Figure 1(f) with Figure 2, nearest interpolation, linear interpolation and spline interpolation have introduced secondary metal artifact with same $k = 0.3$. As can be see from Figure 2 arrowhead.

Figure 3 shows the varieties of 2D CT image with scaling coefficient k in the polynomial-based fit metal artifact reduction algorithm. From left image to right image is $k = 0.0$, $k = 0.1$ and $k = 0.5$, respectively.

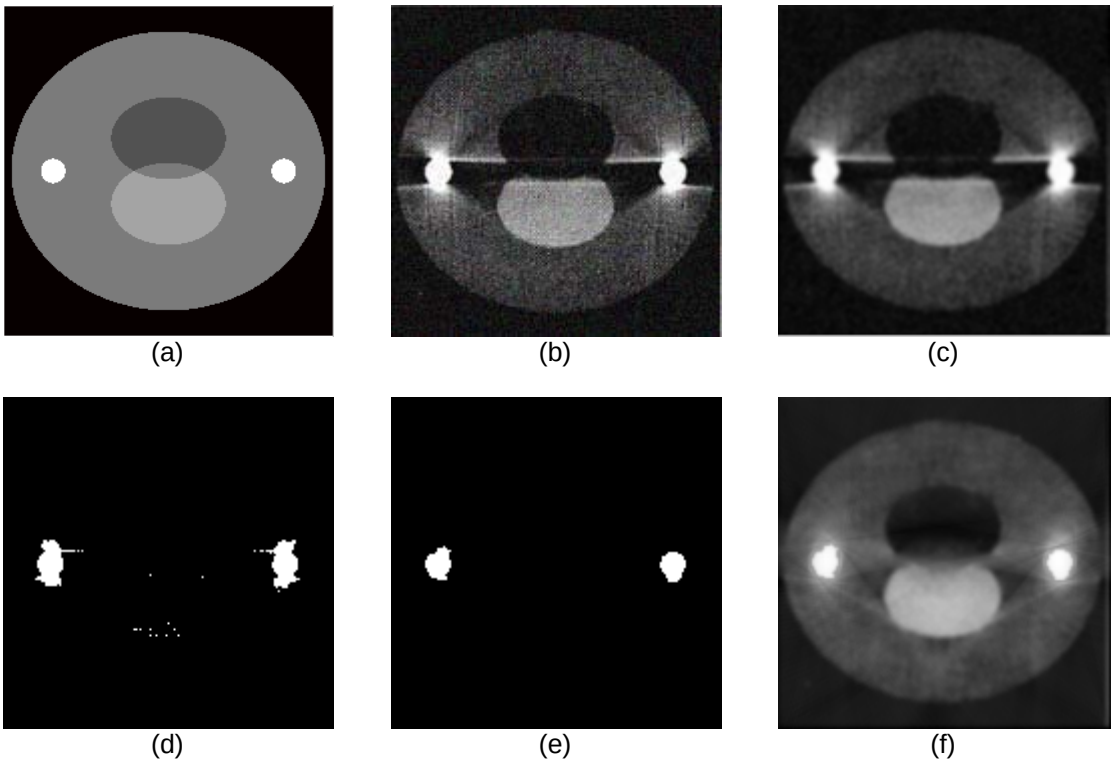

(a) (b) (c)

(d) (e) (f)

Figure 1. Proposed Algorithm Course. (a) Idea model (b) Original 2D cross-section image (c) Filtered image (d) Coarsely segmented image (e) Nearly accurate segmentation image (f) Corrected image

3.3. Algorithms Compare

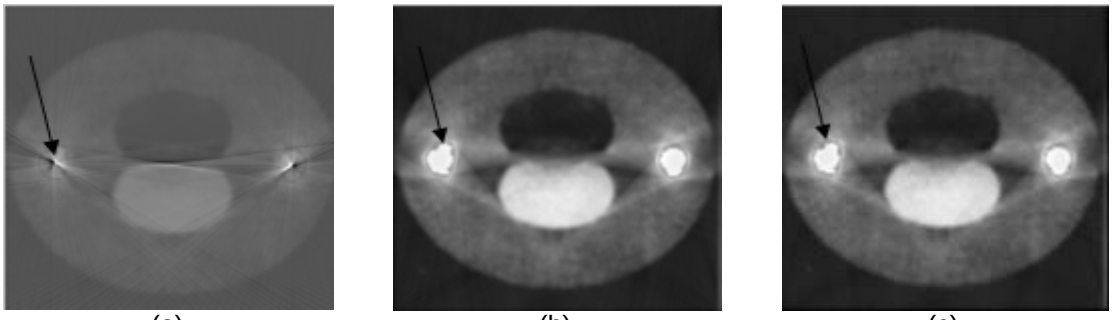

(a) (b) (c)

Figure 2. Different Algorithms Compare. (a) Nearest interpolation, (b) Linear interpolation and (c) Spline interpolation

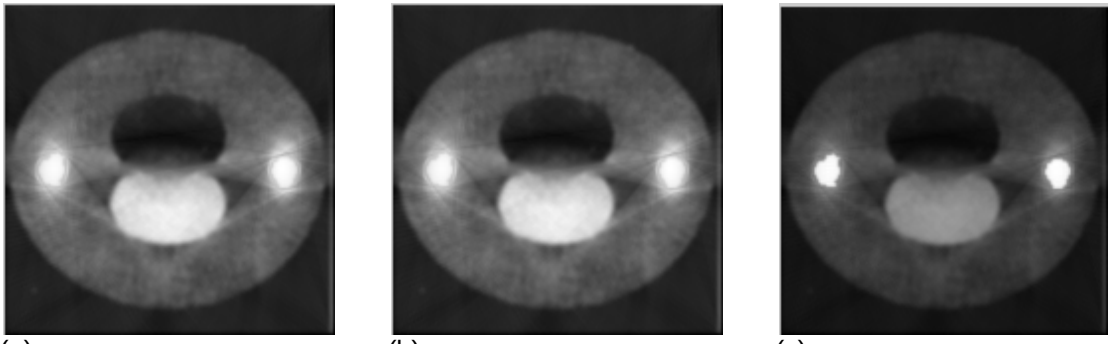

(a) (b) (c)

Figure 3. Polynomial-based Fit Algorithms Compare with Different Scale Coefficient k . (a) $k = 0.0$. (b) $b = 0.1$. (c) $k = 0.5$

Figure 4(a1) and Figure 4(a2) show the projection sinograms of Figure 1(c) and Figure 1(f), respectively. To thoroughly examine the cause of the metal artifacts, the profiles of the x-ray attenuation at rotation angles $\theta = 20^{\circ}$ are plotted in Figure 4(b1). The corrected profiles are shown Figure 4(b2).

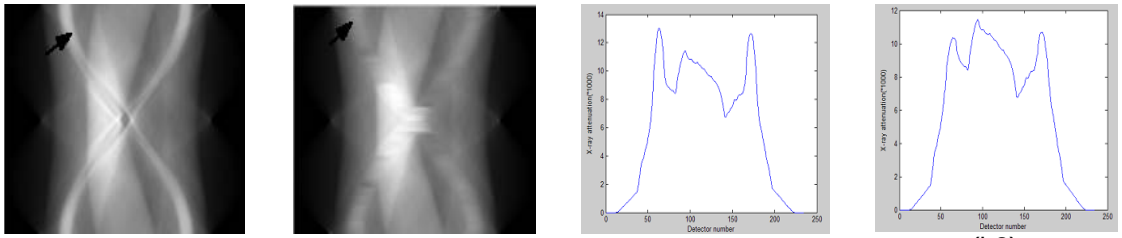

(a1) (a2) (b1) (b2)

Figure 4. Compare with Uncorrected and Corrected. (a1) Projection of Figure.1 (b). (a2) Corrected projection. (b1) Uncorrected profiles of $\theta = 20^{\circ}$. (b2) Corrected profiles of $\theta = 20^{\circ}$

3.4. Validation Methods

To further demonstrate the validation and feasibility of the proposed MAR algorithm, the authors used two methods with the names of Root Mean Square Error(RMSE) and Signal to

noise ration (SNR), respectively. The characters (11) and (12) show their corresponding formulae.

$$ERROR_{RMS} = \frac{1}{I * J}\sqrt{\sum_{i=1}^{I}\sum_{j=1}^{J}(g(i,j) - f(i,j))^2} \tag{11}$$

$$SNR = 10\log_{10}\left[\frac{\sum_{i=1}^{I}\sum_{j=1}^{J} g(i,j)^2}{\sum_{i=1}^{I}\sum_{j=1}^{J}[g(i,j) - f(i,j)]^2}\right] \tag{12}$$

Where $g(i,j)$ is the ideal model image and $f(i,j)$ is no-ideal model image. Table 2 and Table 3 show the RMSE and SNR between Figure 1(a) and Figure 1(c), Figure 1(f) and Figure 2, respectively.

Table 2. RMSE Comparison

Figure.1(a) and Figure.1(c)	Figure.1(a) and Figure.1 (f)	Figure.1(a) and Figure.2(a)	Figure.1(a) and Figure.2(b)	Figure.1(a) and Figure.2(c)
0.32618	0.20912	0.33252	0.24257	0.26791

Table 3. SNR Comparison

Figure.1(a) and Figure.1(c)	Figure.1(a) and Figure.1 (f)	Figure.1(a) and Figure.2(a)	Figure.1(a) and Figure.2(b)	Figure.1(a) and Figure.2(c)
8.451	16.532	8.634	14.762	15.913

As can be seen from Table 2, the RMSE is 0.32618 between Figure 1(a) and Figure 1(c). By using the nearest interpolation, linear interpolation, spline interpolation and the proposed methods, the RMSEs are gradually becoming smaller from 0.33252, 0.24257, 0.26791 to 0.20912. Correspondingly, the SNRs progressively increased from 8.451, 8.634, 14.762, 15.913 to 16.532 in the Table 3.

4. Conclusion

In this paper, the authors presented a novel algorithm to reduce metal-induced artifacts caused by beam hardening, scattered radiation and quantum noise. The algorithm is a region-based maximum value and polynomial-based fit technology. Firstly, maximum value search is used to accurately segment the metal object from the coarsely segmented image. Then, the projection data of every row is fit by different polynomial. Finally, according to the corresponding polynomial and the coordinates of columns, the values of corrupted region of projection data in the row is computed and inserted into the corrupted region of projection data. Phantom study has demonstrated that the proposed algorithm can effectively suppress or remove the streak metal artifacts. Moreover, the proposed algorithm can achived better effect than those of classical methods.

References

[1] Barbel Kratz, Imke Weyers, Thorsten M. Buzug. A fully 3D approach for metal artifact reduction in computed tomography. *Medical physics*. 2012; 39(11): 7042-7054.
[2] Douglas D Robertson, Peter J. Wiess, Elliot K Fishman, et al. Evaluation of CT Techniques for Reducing Artifacts in the Presence of Metallic Orthopedic Implants. *Journal of Computer Assisted Tomography*. 1988; 12(2): 236-241.
[3] P Seitz, P Ruegsegger. CT bone densitometry of the anchorage of artificial knee joints. *Journal of Computer Assisted Tomography*. 1985; 9(3): 612-622.

[4] JA Veiga-Pires, M Kaiser. Artifacts in CT scanning. British Journal of Radiology. 1979; 52(614): 189-204.
[5] Nogah Haramati, Ronald B Staron, Mazel-Sperling K, et al. CT scans through metal scanning technique versus hardware composition. *Computerized Medical Imaging and Graphics*. 1994; 18(6): 429-434.
[6] Li Y, Chen Y, Luo L, Zhang P, Zhang Q. Fast CT metal artifacts correction based on derivative and region-based filling. *Journal of medical imaging and radiation oncology*. 2011; 55(6): 535-541.
[7] W A Kalender, R Hebel and J Ebersberger. Reduction of CT artifacts caused by metallic implant. *Radiology*. 1987; 164(2): 576-577.
[8] Veldkamp WJ, Joemai RM, vander Molen AJ, Geleijns J. Development and validation of segmentation and interpolation techniques in sinograms for metal artifact suppression in CT. *Medical physics*. 2010; 37(2): 620-628.
[9] Verburg JM, Seco J. CT metal artifact reduction method correcting for beam hardening and missing projections. *Physics in Medicine and Biology*. 2012; 57(9): 2803-2818.
[10] Esther Meyer, Rainer Raupach, Michael Lell, et al. Frequency split metal artifact reduction (FSMAR) in computed tomography. *Medical physics*. 2012; 39(4): 1904-1916.
[11] Hua Li, Camille Noel, Haijian Chen, H Harold Li. Clinical evaluation of a commercial orthopedic metal artifact reduction tool for CT simulations in radiation therapy. *Medical physics*. 2012; 39(12): 7507-7517.
[12] F Edward Boas, Dominik Fleischmann. Evaluation of Two Iterative Techniques for Reducing Metal Artifacts in Computed Tomography. *Radiology*. 2011; 59(3): 894-902.
[13] Katrien Van Slambrouck, Johan Nuyts. Metal artifact reduction in computed tomography using local models in an image block-iterative scheme*. Medical physics*. 2012; 39(11): 7080-7093.
[14] Daniel Prell, Yiannis Kyriakou and Willi A Kalender. Comparison of ring artifact correction methods for flat-detector CT. *Physics in Medicine and Biology*. 2009; 54(12): 3881-3895.
[15] Daniel Prell, Yiannis Kyriakou, Willi A Kalender. A dedicated raw data-based metal artifact reduction method for flat-detector CT. *European Radiology*. Vienna, Austria. 2009; 19(257).
[16] Abdolvahab Ehsani Rad, Mohd Shafry Mohd Rahim, Alireza Norouzi. Digital Dental X-Ray Image Segmentation and Feature Extraction. *TELKOMNIKA Indonesian Journal of Electrical Engineering*. 2013; 11(6): 3109-3114.
[17] Jun Lai, Mei Xie. Automatic Segmentation for Pulmonary Vessels in Plain Thoracic CT Scans. *TELKOMNIKA Indonesian Journal of Electrical Engineering.* 2013; 10(4): 743-751.
[18] Mehran Yazdia, Luc Gingras, Luc Beaulieu. An adaptive approach to metal artifact reduction in helical computed tomography for radiation therapy treatment planning: experimental and clinical studies. Int. *J. Radiation Oncology Biol. Phys*. 2005; 62(4): 1224–1231.
[19] Laigao Chen, Yun Liang, George A Sandison, et al. A novel method for reducing high attenuation object artifacts in CT reconstructions. *SPIE.* 2002; (4684): 841-850.